2022

# Developing a Nasal Organotypic Model to Investigate the Effects of the Nasal Microbiome on the Susceptibility to Pathogens

Victor Lam

# Developing a Nasal Organotypic Model to Investigate the Effects of the Nasal Microbiome on the Susceptibility to Pathogens

Victor Lam

Supervisor: Dr. Jessica Prodger

**Abstract.**

The nasal mucosa is colonized by diverse bacteria, however, the influence of the nasal microbiome on the susceptibility of respiratory pathogens in adults is poorly understood. Defining the complex relationship requires a relevant *in vitro* model, but current nasal models fail to differentiate into a pseudostratified columnar epithelium that mimics the nasal milieu. Hence, these models can not support the investigation of these aspects concurrently. In this study, we established an *in vitro* human primary nasal epithelial model using the air-liquid interface (ALI) condition. Commercially available and locally isolated nasal cells were successfully differentiated into pseudostratified columnar epithelia. The differentiated epithelium included goblet and ciliated cells as indicated by an enzyme-linked immunosorbent assay and immunofluorescence imaging. Notably, I have identified visual ciliary beating (viewed under light microscopy) as a simple and accessible method of indicating cell differentiation and polarization. This finding is further supported by reverse transcription-quantitative polymerase chain reaction results on angiotensin-converting enzyme 2 (ACE2) and transmembrane serine protease 2 (TMPRSS2) expression and by severe acute respiratory syndrome coronavirus 2 (SARS-CoV-2) viral challenges. Compared to the ALI model with no ciliary motion (ALI-N), the ALI model with ciliary beating (ALI-C) demonstrated an increased expression of ACE2 and TMPRSS2. The increased gene expression resulted in greater permissiveness to SARS-CoV-2 infection observed as greater luciferase intensity. Interestingly, the submerged undifferentiated model exhibited phenotypes and functional characteristics comparable to the ALI-N. However, both conditions failed to differentiate and support viral infection. Our results highlight the importance of primary nasal cells to develop a differentiated model to support viral challenges Thus, this study provides a fundamental model for future viral-microbiota-host interaction studies.

**Introduction.**

The human microbiome is an essential component to the health and functioning of the immune system. The microbiome composition has been linked to many diseases and can regulate multiple aspects of the immune system. For example, antibiotic usage, which disturbs the gut microbiome, has been associated with an increased risk of *Clostridium difficile* infection[1]. We have previously shown that an anaerobic dysbiosis of the penile microbiome can alter local immune responses, associated with an increased risk of human immunodeficient virus susceptibility[2]. Similar to the penile microbiome, the nasal mucosa hosts diverse bacteria that may alter nasal immune responses. As the first line of defense against respiratory pathogens, the nasal epithelium secretes innate immune molecules such as mucus, interferons (IFNs), and antimicrobial peptides (AMP). These defense molecules have anti-viral and anti-bacterial properties[3–5], and can be influenced by bacteria colonized on the nasal surfaces. It has been shown that the colonization of nasal *Staphylococcus epidermidis* stimulated the secretion of AMPs and increased the production of IFN-λ in nasal epithelial cells[6,7]. The nasal *S. epidermidis*-stimulated IFN-λ expression prevented pulmonary spread of influenza A virus in mouse models[7]. Likewise, individuals colonized with *Streptococcus spp* were observed to have a reduced susceptibility to influenzas A and B[8]. Hence, commensal bacteria that enhance anti-viral responses may confer resistance to respiratory viral infections. Our collaborator, Dr. Cindy Liu, has identified seven distinct community state types (CST), defined by key indicator species, in the adult nasal microbiome of Danish adults[9] (see Supplemental Figure 1). However, the connection between the nasal **microbial composition** and its effect on nasal immune responses relevant to adult respiratory viral infection, is poorly understood.

Determining the relationship and the influence between the host, nasal microbiota, and respiratory pathogens is crucial for identifying novel preventative strategies against an increasing number of pathogens. Due to the lack of experimental studies investigating these aspects concurrently, a novel *in vitro* model could serve to control the nasal CSTs, the exposure to pathogens of interest, and host variability. An *in vitro* model must accurately differentiate keratinocytes into phenotypes with cellular receptors that mimic *in situ* tissues to translate findings. The pseudostratified columnar epithelium is the desired phenotype as seen in nasal mucosae, consisting of goblet cells and ciliated columnar cells. Goblet cells in the respiratory tract produce mucus that is rich in mucin. Mucin proteins form a gel-like secretion that traps pathogens and prevents their invasion into the host epithelium[10,11]. In the airway, MUC5AC and MUC5B predominate the composition of mucus. MUC5AC, is secreted by goblet cells only, whereas MUC5B is released by submucosal glands[12–14]. Ciliated cells and mucus work together to facilitate pathogen clearance. These ciliated cells have beating cilia that propel the mucus upward to the nasal cavity for removal[15]. The differentiation of keratinocytes into these specialized ciliated columnar and mucus-producing goblet cells can be performed *in vitro* using the air-liquid interface (ALI) condition. The ALI condition is achieved using transwell inserts where the cells adhere to the insert membrane placed inside a 24-well transwell. This setup creates two compartments, the apical surface, which exposes the culturing nasal epithelium to air, and the basolateral surface, which feeds the epithelium with media. The ALI condition is introduced by removing the apical media while maintaining the basolateral media. This air-interface condition triggers keratinocytes that are in contact with air to differentiate[16]. In contrast, cells cultured in a liquid-liquid interface (LLI), which lack apical contact with air, remain undifferentiated. As a result, these LLI cells fail to exhibit mucociliary function[17]. Of equal importance, cellular receptors must also reflect ones

observed *in situ* tissues to investigate the viral-microbiome interaction in the nasal mucosa. The differentiation states of nasal cells during viral infection have critical implications in determining viral susceptibility. Severe acute respiratory syndrome coronavirus (SARS-CoV) and SARS-CoV-2 use the angiotensin-converting enzyme 2 (ACE2) receptor, with the aid of proteolytic processing by transmembrane serine protease 2 (TMPRSS2), to enter and infect ciliated cells[18]. ACE2 receptors are polarized to the apical side in differentiated cells only, and trafficking of ACE2 receptors to the cellular membrane enables greater SARS-CoV susceptibility[19]. In contrast, undifferentiated cells are poorly infected by SARS-CoV due to the minimal ACE2 expression in the apical surface[19]. Similarly, TMPRSS2 is highly expressed at the apical surface in differentiated nasal epithelium[18]. Therefore, mucociliary differentiation of nasal keratinocytes *in vitro* is crucial in developing a representative nasal epithelial replica.

Current options for nasal models for investigating the host-bacterial-viral interactions include the use of human nasal cancer cell lines, human non-cancerous cell lines, or human primary nasal epithelial cells (HpNECs)[17–23]. Of the human cancer cell lines, the Calu-3 and the RPMI-2650 cells were derived from lung adenocarcinoma and squamous cell carcinoma, respectively[24–26]. Due to their cancerous properties, these cells are capable of indefinite proliferation without the issue of cell senescence seen in primary cells, but cancerous cell lines are not without limitations. These cancer cell lines do not recapitulate immune defenses nor phenotypes exhibited by *in vivo* epithelia. For example, when exposed to enterotoxin B, the Calu-3 cell line had increased production of interleukin-6 (IL-6) and IL-8 that were not observed in primary cells[20]. Regarding phenotypic differentiation, the RPMI-2650 cell line has been shown to produce undifferentiated, squamous cells[21]. Likewise, the Calu-3 cell line failed to exhibit cilia differentiation *in vitro* despite being cultured in the ALI condition[22]. Human non-cancer cell lines include the

HBEC3-KT and VA10 cell lines. These are created by immortalizing primary bronchial cells with oncogenic genes to extend proliferative capacity. The HBEC3-KT cells require the CDK4 gene to prevent telomere-independent growth arrest and the hTERT gene to compensate for the loss of telomeres—both genes function to block cell senescence and increase the number of cell-doubling [23]. Nonetheless, HBEC3-KT in the ALI condition is an unrepresentative model of the respiratory epithelium due to the formation of immotile cilia[27]. Finally, HpNECs are isolated from donors and stored without genetic modifications. Unlike other cell lines, primary cells differentiate into pseudostratified epithelia in the presence of the ALI condition and exhibit ciliary beating with MUC5AC production, indicative of goblet cells formation[27–29]. When HpNECs are cultured in the submerged LLI condition, they fail to differentiate and retain a monolayer appearance like cells cultured in flasks[16]. Despite the inevitability of cell senescence, primary cells exposed to the ALI condition closely resemble cells found *in situ* tissues[30], suggesting that HpNECs are accurate and suitable *in vitro* study models.

The development of an *in vitro* model that mimics the nasal milieu is crucial to delineate the influence of the nasal microbiome on viral and bacterial susceptibility, as there are no current models that investigate these aspects together. Therefore, I **hypothesize** that an *in vitro* nasal organotypic model cultured in an air-liquid interface would better approximate *in situ* tissues than undifferentiated cells by exhibiting mucociliary differentiation and permissiveness to SARS-CoV-2 infection. This hypothesis will be tested through the following specific aims. **Aim 1** will compare two cell isolation methods from nasal mucosal tissues and identify the most efficient one based on the yield of viable cells. **Aim 2** will introduce the ALI condition to cells and verify mucociliary differentiation. Finally, **aim 3** will investigate the success of ALI and submerged models to support the SARS-CoV-2 viral challenge.

## Materials and Methods.

### Ethics Statement.

This cross-sectional and anonymous study to obtain nasal turbinate tissues, treated as a part of patients' otolaryngological surgery, was approved by the Western University Health Science Research Ethics Board and the Lawson Health Research Institute (Western protocol number: 119682, Lawson's protocol number 11602). The donated tissues were used to isolate human nasal epithelial cells to generate *in vitro* cultures to study nasal-bacterial-viral interactions. Adults (18 years and older) scheduled to undergo otolaryngological surgery were invited by the head and neck surgeon Dr. Leigh Sowerby to participate in our study voluntarily. Written consent was provided for tissue collection prior to the surgery. The sample tissues were non-identified as no participants' information was associated with them. Only the anatomical location and the visible state (inflamed or non-inflamed) of the tissue were labelled. A unique study number was generated at the laboratory once samples had been transported to Western University from either the University's hospital or St. Joseph's healthcare London.

### Establishing a Nasal Organotypic Model.

### Isolation of Human Primary Nasal Epithelial Cells (HpNECs).

The upper airway tissues were obtained from patients undergoing otolaryngological surgery. Tissues were collected from the superior, middle, and inferior turbinate. Two methods were used to isolate HpNECs from collected tissues. First, the "Crawl-Out" method allows small pieces of tissue to adhere to a plate before epithelial cells migrate out from the original tissue for cell harvest. The Crawl-Out method was modified from a current protocol[17]. Tissues were placed in a 50 ml falcon tube (Fischerbrand, Waltham, Ma, USA) and washed by adding 40 ml of 1X

Dulbecco's phosphate-buffered saline (D-PBS, Wisent Inc, QC, Canada). The tubes were centrifuged at 1500 rpm for 8 mins, and the supernatant was discarded before a second wash. Then, the tissues were incubated in 0.25% Trypsin/EDTA (Sigma-Aldrich, St. Louis, MO, USA) for 10 minutes at 37°C with 5% CO2 supplemented air. Next, tissues were cut into smaller pieces of about 0.2 $cm^3$ in length and placed into a 6-well plate that was submerged in 1 ml of 1x Keratinocyte Serum-Free Media (KSFM, Gibco, Waltham, MA, USA) with 4% Primocin (InvivoGen, San Diego, CA, USA). Upon reaching confluency near the tissue, cells were harvested using Accutase™ (Sigma, Burlington, MA, USA), incubated for 8 mins at 37°C in 5% CO2 supplemented air, then harvested cells were plated onto a six-well transwell. Tissues were refed with media to continue cell propagation. The second method, the "Dispase" method utilizes dispase enzymes to directly detach the epidermis before collecting isolated cells. The Dispase method was performed using a modified protocol[29,31]. After the centrifuge washes mentioned above, tissues cut into smaller pieces of about 0.2 $cm^3$ were placed in a 6-well plate and incubated in dispase (1.82 U/ml, Gibco) overnight at 4°C. Dispase was inactivated with Dulbecco's Modified Eagle Medium (DMEM, Gibco) with 10% fetal bovine serum (FBS, Sigma) and cartilage was removed from the epithelium. Next, tissues were placed into a 50 ml flacon tube and diced into fine pieces before 0.25% tryspin/EDTA incubation for 10 minutes while ensuring the volume of trypsin covered the tissues. Neutralization was performed with 3-volume equivalents of Trypsin/EDTA with DMEM+10% FBS. Then, the solution was passed through a 70 µm nylon cell strainer (Fischerbrand) to collect isolated cells. Collected cells were centrifuged at 1500 rpm for 5 mins before resuspending in KSFM. Suspended cells were plated onto a 6-well plate. The fine pieces of tissues collected by the cell strainer were plated similarly to the Crawl-out method to determine whether cells would continue to migrate after the Dispase protocol. The recovery of

viable epithelial cells is used to compare and identify the optimal isolation protocol. Viable epithelial cells are measured by minimal fibroblast contamination and the success of expanding these cells cultures from a six-well plate to an ALI model.

**Cell Culture.**

Prior to the approval of tissue collections, commercially available HpNECs were purchased from Promocell (Heidelberg, Germany). Nonetheless, methods for culturing HpNECs are identical regardless of the origin of the cells. Cells were grown in T-25 flasks using Airway Epithelial Cell Growth Media (AECGM; Promocell) with provided supplements at 37°C with 5% CO2 and changed every other day. Incubation of Accutase™ for 6 minutes was performed to detach cells from the flask. For strongly adherent cells, 0.05 mM of EDTA/PBS was incubated for 5 minutes prior to the Accutase™ treatment. Next, 1.5 x $10^5$ cells/$cm^2$ were seeded on a 24-well transwell (PET membrane, 0.4 μm pore size, Fischer Scientific, Waltham, Ma, USA). At 100% confluency, the apical media was removed to introduce the ALI condition while the basolateral media was replaced by the ALI media (Promocell) with supplements. The media was changed every 3 days. To create the undifferentiated model, 1.5 x $10^5$ cells/$cm^2$ were also seeded into a 96-well flat-bottom plate (WPI, Sarasosa, FL, USA) and the media was changed every 3 days with no introduction of the ALI condition.

To evaluate the optimal culturing media to sustain the cell culture for up to 21 days, AECGM:DMEM (1:1) with AECGM supplements and 10% FBS was used as the differentiation media to compare cell differentiation with the ALI media from Promocell.

**Bright-Field Microscopy.**

To visualize the confluency of cell cultures, bright-field microscopy (Axio Observer A1 inverted microscope, Zeiss, Oberkochen, Germany) was used. Additionally, the ALI models were

examined under bright-field microscopy to capture the differentiating epithelium every 3 days under 50x total magnification. Finally, ciliary motion was observed under 400x total magnification.

**Organotypic Model Characterization.**

**MUC5AC ELISA.**

To characterize the differentiation of the nasal model, the MUC5AC sandwich enzyme-linked immunosorbent assay (ELISA, Biomatik, Kitchener, ON, Canada) was performed to determine the presence of goblet cells. 40 µl of PBS was added to the apex of the transwell and incubated for 5 minutes in room temperature to collect mucus on the apical surface every 3-4 days during the ALI condition. MUC5AC in PBS solution was stored at -20°C. The ELISA was used according to the manufacture protocol. Ten µl of the collected mucus was added to the ELISA plate and mixed with 90 µl of the provided diluent to achieve a total dilution of around 400-fold. Cytation 5 microplate reader (Biotek, Winooski, VT, USA) was used to detect light emission at 450 nm wavelength.

**Immunofluorescent Microscopy.**

To visualize the differentiation state of the nasal model, immunofluorescent microscopy was used to assess the presence of goblet cells and cilia formation. At 21 days post-ALI, 100 µl of PBS was added to wash the insert 3 times before fixing it with 3.7% paraformaldehyde in PIPES buffer for 15 minutes. Next, 100 µl of donkey blocking buffer (10% Normal Donkey serum, 0.1% Triton X-100, and 0.01% NaN3) was added and incubated at room temperature for 30 mins. Fixed cells were incubated with conjugated antibodies for 1 hr at 37°C. A dilution series diluted with donkey blocking buffer were performed at dilutions of 1:100, 1:200, 1:400, and 1:800 for each

antibody to determine the optimal dilution. Mouse Alexa flour®-647 conjugated MUC5AC antibodies (SCBT, Dallas, Tx, USA) and mouse Alexa Flour®-488 conjugated acetylated-alpha tubulin antibodies (SCBT) were used to identify MUC5AC and cilia, respectively. Following antibody incubation, cells were washed three times with 100 µl of PBS. Cells were only washed after fixation occurred to minimize the disruption of the cell layer. Then, the insert membrane was carefully removed using a scalpel, and the membrane was mounted on a ColorFrost Plus glass microscope slide (Fisherbrand) using Fluoromount G mounting media with DAPI (Thermo Fisher, Waltham, Ma, USA) to counterstain for nuclei. Finally, whole tissue section scans were taken at 20x magnification using a DM5500B fluorescence microscope (Leica Camera Ag, Wetzlar, Germany).

**Establishing ALI Condition as a Better *in vitro* Model than Undifferentiated Cells.**

**ACE2 and TMPRSS2 RT-qPCR.**

To investigate the polarization of the ALI nasal model and the permissiveness of SARS-CoV-2 infection in comparison to undifferentiated cells, reverse transcription-quantitative polymerase chain reaction (RT-qPCR) was performed. At 21 days post-ALI with or without visible ciliary motion, cells were isolated from the inserts using a cell scrapper and stored in RNA-later (Invitrogen, Waltham, Ma, USA) at -20°C. To standardize the number of cells throughout the process, cells from 2 inserts or wells were combined to create one sample. Qiagen RNeasy mini kit (Qiagen, Hilden, Germany) was used to isolate total mRNA according to the manufacturer's instructions, and Nanodrop™ 2000/2000c spectrophotometer (Thermo Fisher) was used to verify the purity of the RNA to be ~2.0 in A260/280 readings. The iSCRIPT cDNA synthesis kit (Biorad, Hercules, CA, USA) was used to obtain total cDNA. Next, the TaqMan gene expression assay

(Thermo Fisher) was used to quantify the relative abundance of ACE2 (assay ID: Hs01085333_m1) and TMPRSS2 (assay ID: Hs01122322_m1) in differentiated and undifferentiated cells based on previous publication[32]. A single-plex TaqMan expression assay was performed with the housekeeping gene RPS-18 provided by our collaborator Dr. Cindy Liu according to previous work to identify a reliable housekeeping gene[33]. Using the Fast advanced master mix (Thermo Fisher), a fast plate qPCR was performed and the QuantStudio 5 (Thermo Fisher) was used to detect fluorescence. See supplemental Table 1 for the primer and probe sequence of the housekeeping gene.

**Infection Model.**

To compare the susceptibility of SARS-CoV-2 infection between the nasal ALI model and the submerged, undifferentiated model, a wild-type SARS-CoV-2 Nanoluciferase (SARS-CoV-2 nLuc) viral challenge was performed. The infection process was performed by Dr. Kate Parham in Dr. Ryan Troyer's laboratory. HpNECs cultured on 24-well transwells in ALI conditions and 96-well plates in submerged conditions were inoculated with 100 µl of the viral inoculum on day 5 and day 26 post-ALI. The viral stock was diluted in PBS to achieve an MOI of 1 (75,000 TCID50) and MOI of 0.1 (7500 TCID50). The viral inoculum was added to the cells and incubated for 1 hr before discarding it. Then, the cells were incubated for 3 days at 37°C + 5% CO2 supplemented air. After 3 days, 50 µl of PBS was added to the cells and mixed with 50 µl of Nano-Glo® Luciferase Assay Reagent (Promega, Madison, WI, USA) for optimal consistency. Then, 80-90 µl of the mixture were transferred into a black 96 well plate. Finally, a 3-minute wait period was necessary prior to detecting the luminescence on a microplate reader, Cytation 5 (Biotek).

## Results.

### Clinical Data.

To obtain clinical samples for cell isolation, I prepared an ethics proposal which included contacting a head and neck surgeon to collaborate in our study, identifying the inclusion criteria for healthy patients, and drafting the study plan and rationale for this project. The inclusion criteria included the recruitment of adult patients, 18 years of age or older, undergoing sinus and base skull surgery for non-inflammatory indicators occur in-person during pre-surgical consultation by the surgeon. This anonymous tissue collection only collected information on the anatomical location of the tissue and the visible inflammation of the tissue. The gender of the participants was not considered, as the primary goal of the project was to isolate cells from tissues. To date, samples were collected from nine participants (Table 1). Tissues that arrived at the laboratory were immediately processed in one of the two methods (Crawl-out or Dispase method).

### Cell Isolation.

To determine the most efficient manual cell isolation method from nasal samples, both Crawl-Out and the Dispase methods were used. In the Crawl-Out method, cells began to migrate outwards from the tissue mass, seven days post-cell isolation. By 10 days, cells were ready to be harvested as shown in Figure 1. The tissues were capable of three to four rounds of cell harvesting prior to the cessation of cellular proliferation. In comparison, the Dispase method yielded cells immediately that were ready to be passaged three days after the isolation protocol (Figure 2). However, the Dispase method prevents the chance for multiple harvests performed in the Crawl-Out protocol. To overcome this barrier, tissues that underwent the Dispase method were also introduced to the Crawl-Out method by adhering the fine pieces of tissue onto the plate (Figure 3).

Although cells could be harvested using this third method (Dispase + Crawl-out), greater cell death occurred in later passages which prevented cell cultures to be expanded to the ALI model. In general, cells processed through the Crawl-Out method seemed to have greater difficulty reattaching to plates after cell harvests compared to the Dispase method. As seen in sample HNEC_003, the Dispase cell isolation process was successful in establishing an ALI and submerged model. These results suggest that both methods were successful in cell isolation. The Dispase method demonstrated rapid isolation for establishing the ALI model; the Crawl-out method was slower but generated a stable supply of cells up to four harvests.

**ALI and Submerged Models.**

To establish a nasal organotypic model, commercially available cells and cells isolated from tissue samples were used. In addition, two media, AECGM:DMEM and ALI media, were used to investigate their effects on epithelial stability. The use of either source of cells provided successful ALI models as observed by light microscopy. Cells exposed to the ALI condition after reaching confluency were maintained for up to 27 days using either AECGM:DMEM or ALI media as the differentiation media. These successful cultures created an interesting epithelial topography visible under light microscopy (Figure 4A-F) and ciliary beating was visible by mucus transport at D18 post-ALI under 400x magnification using a bright-field microscopy. However, using the ALI media as the differentiation media resulted in quicker cell differentiation in comparison to the AECGM:DMEM media. This rapid differentiation led to an accelerated visible ciliary motion as seen four days post-ALI. In instances where air-interfacing was introduced prior to 100% confluency, gradual cell death (Figure 5) occurred with no ciliary motion.

Similarly, commercially available cells or isolated cells successfully created the submerged model and there were noticeable differences between the submerged and the ALI model. In the submerged model, the phenotype exhibited by undifferentiated cells was identical to that of cells cultured in normal flasks. Secondly, submerged cells formed a monolayer, unlike the topography seen in ALI models. Finally, these cells were only maintained up to two weeks before cell death began.

Interestingly, it was observed that some cells cultured under the ALI condition either developed visible ciliary motion or lacked ciliary beating. To further investigate ciliary beating under light microscope, we grouped the cells into three categories based on the presence of visual ciliary motion and the culturing condition. Cells that underwent the ALI condition with ciliary beating is known as ALI-C and cells that underwent the ALI condition yet lack ciliary motion is referred to as ALI-N. Finally, cells that were left submerged in media is known as submerged or undifferentiated cells and as expected, these cells did not produce ciliary motion.

**Assessing ALI differentiation.**

**Immunofluorescence.**

To assess the differentiation state of the ALI model, immunofluorescence microscopy was used to detect the presence of goblet cells and cilia formation. Anti-Acetylated-α tubulin antibodies were used to stain stable microtubule that would be indicative of cilia formation and Anti-MUC5AC were used to stain for goblet cells as only goblet cells secret MUC5AC mucins. At 1:400 dilution, red fluorescence signals were detected indicative of goblet cell formation (Figure 6A). At 1:800 dilution, distinct green fluorescence was observed, indicating the presence of ciliated cells (Figure 6B). DAPI was used to counterstain and the presence of blue fluorescence

indicates nucleated cells. The appearance of these cellular characteristics suggests a successful pseudostratified epithelial differentiation.

**MUC5AC ELISA.**

To further access the presence of goblet cells in the differentiated ALI model, MUC5AC ELISA was performed. Goblet cells were indicated to be present in the ALI-C model as depicted by MUC5AC ELISA. MUC5AC concentration appeared to increase, peaking at day 21 post-ALI condition before decreasing until day 27 when the culture was terminated (Figure 7).

The immunofluorescence and ELISA results suggest cells that have undergone the ALI condition demonstrate the characteristics and phenotype of a pseudostratified columnar epithelium found in the nasal milieu.

**ALI Model in Comparison to Undifferentiated cells**

**RT-qPCR.**

To utilize the ALI model for viral interaction studies, the susceptibility of the model was assessed by qPCR for the presence of the viral receptor ACE2 and the protease TMPRSS2. ALI-C models and ALI-N models were compared to the submerged, undifferentiated model. The ALI-C models showed the highest relative expression of TMPRSS2 and ACE2 compared to the model that underwent the ALI condition but had no ciliary motion and the submerged condition. Interestingly, although the ALI-N model showed higher relative abundance for both genes of interest than the submerged condition, the two conditions are relatively similar (Figure 8). The ALI condition with visible ciliary motion exhibited a 543.3-fold increase in TMPRSS2 expression compared to the submerged condition. Likewise, ACE2 expression was increased by 134.4-fold in

the ALI-C condition compared to submerged models (Figure 9). These qPCR results suggest that cell differentiation is crucial in the polarization and upregulation of ACE2 and TMPRSS2 genes.

**SARS-CoV-2 Infection Model.**

To further highlight the utilization of the nasal ALI model, wild-type SARS-CoV-2 nLuc viruses were used to infect the ALI and submerged models in collaboration with Dr. Kate Parham. Compared to the no-virus condition, there was an increase in luciferase intensity with an increased multiplicity of infection in the ALI-C models (Figure 10A). In the second round of the viral challenge, the ALI-N model exhibited a slight increase in luciferase intensity compared to the submerged cells. However, this increase in luciferase intensity was not as drastic as the ALI-C model (Figure 10B). Compared to the ALI-N model, ALI-C model had a 22-fold greater luciferase intensity. Compared to submerged cells, the ALI-C model had a >300-fold increase in luciferase intensity. This infection data suggest that the differentiation state of the nasal model is crucial for the permissiveness of SARS-CoV2, and these results concord with the qPCR data.

**Discussion**

The upper respiratory epithelium is the first line of defense against life-threatening respiratory pathogens like SARS-CoV-2. An accurate *in vitro* nasal model of the nasal epithelium remains necessary to study the pathogenesis and treatment for respiratory illnesses. In this study, we established an *in vitro* nasal organotypic model through the ALI condition that differentiated cell cultures into goblet and ciliated cells matching the pseudostratified columnar epithelial cell phenotype. The ALI model was shown to be a better *in vitro* model compared to undifferentiated, submerged cells. Furthermore, to our knowledge, no other studies have used visual ciliary motion under bright microscopy as an indicator of cell differentiation. This was supported by the SARS-

CoV-2 challenge where cells lacking ciliary beating, both ALI-N and submerged cells, had unsuccessful viral infections. This study demonstrates the importance of the differentiation state achieved by primary cells in the ALI condition and this model is crucial for future viral-bacterial-host interaction studies.

The visualization of cilia motion under the bright-field microscope in ALI models is shown to be a good indicator of terminal cell differentiation. Previous studies have captured ciliary beating using specialized cameras[34,35], however, we present a more accessible signal of cell differentiation with a light microscope. Although ciliary beating occurs only after exposure to the ALI condition, and submerged cells completely lack this visual indicator, further confirmation of ciliary presence is needed. Immunofluorescence microscopy detected acetylated-α tubulin stain in the ALI with cilia condition, but this was limited by the lack of staining for the ALI-N and the submerged conditions. In addition, the captured IF images could not clearly distinguish the cell phenotype or the location of the acetylated-α tubulin stain. This was because stable microtubules in the cytoplasmic skeleton are also acetylated at lysin-40[36,37]. Furthermore, the lack of cross-sectional imaging of our model hinders a clear depiction of the presence of cilia. Even in cross-sectional images of the ALI model, acetylated-α tubulin stain is only shown to concentrate below the cell membrane—protruding cilia could not be observed[38]. Therefore, future work will investigate the depiction of cell differentiation in a cross-sectional manner using hematoxylin and eosin stains (H&E). H&E staining can provide further insights into epithelial thicknesses; of greater importance, it can depict cilia protrusion and length[35].

The presence of ciliary motion signals cell differentiation and the readiness of the ALI model to support viral challenges. Mucosal transport appears to align with higher expression of ACE2 and TMPRSS2 and higher infectability by SARS-CoV-2 challenge, further supporting the use of ciliary motion as an indicator of the maturation of the model for viral challenges[17]. The increased expression and polarization of ACE2 and TMPRSS2 at the apical surface is a function of the differentiation state of the model[18]. Upregulation of these genes have been shown to relate to increase apical protein polarization, and hence, the success of the SARS-CoV challenge: the higher the ACE2 and TMPRSS2 expression, the more susceptible the model is to SARS-CoV[19]. This finding was also seen in our ALI-C cells that had greater ACE2 and TMPRSS2 mRNA expression, and a greater luciferase intensity post-SARS-CoV-2 viral challenge. In contrast, our cells cultured in ALI-N cells exhibit phenotypic and functional characteristics comparable to cells in the submerged condition. Like submerged, undifferentiated cells, the ALI model with no ciliary beating is poorly infected due to minimal ACE2 and TMPRSS2 expression[19]. These results support the use of primary cells over alternative options for nasal models like the human cancer cell lines. Despite culturing human cancer cell lines in ALI, they remain undifferentiated or progress into squamous epithelial cells[21,22]. As shown in this and several other studies, undifferentiated cells do not exhibit polarization of functional receptors and fail to exhibit proper phenotypes present in the human airway[17,21,22]. Hence, airway cancer cell lines and other non-cancerous cell lines that fail to differentiate would diminish their applications as *in vitro* viral study models.

A limitation lies in the number of experimental trials for the qPCR and the viral challenge results. For the qPCR data, one sample is comprised of two wells of extracted cells for a total of n=2 samples, but only one experimental repeat was conducted. Likewise, the viral challenge assay was repeated only twice, with n=2 for each condition for the first assay and n=3 for the second

repeated viral challenge. Despite the small size of replicates and experimental repeats, the qPCR and the viral assay results suggest the importance of proper phenotypic differentiation for a representative *in vitro* model. Future experiments will look to increase the replicate size to obtain sufficient data for statistical analyses and repeat these experimental procedures to validate the reproducibility of this model.

The differentiation state of the cells and hence, the presence or absence of ciliary motion may be influenced by the timing of the introduction of the ALI condition. Premature exposure to the ALI condition or the lack of cell confluency of the culture before ALI exposure resulted in decreased culture survival observed as gradual cell death and empty patches in the culture. Confluency is crucial in keratinocytes differentiation as close cell-cell contact triggers their commitment to terminally differentiate[39], besides air-interface exposure[16]. Proper phenotype differentiation is necessary to form goblet cells and ciliated cells. The lack of mucus in the epithelium has been shown to impart cilia beating[40], and this study has demonstrated that ciliary motion is a crucial indicator of differentiated cells. At the early stages of premature ALI exposure, around day one to three post-ALI, cell cultures could be rescued by resubmerging the non-confluent cells in media until confluency before re-exposing them to the ALI condition. This method leads to cell death cessation and achieving cell differentiation. However, resubmerging cells after this window may have signaled the cells to halt differentiation resulting in cells observed in the ALI with no cilia condition. It has been shown that resubmerging cells completely results in a lack of ciliary differentiation and a reduction in ACE2 expression compared to the ALI model[17]. Future work will identify a time course for which resubmerging cells prior to ALI re-exposure is beneficial in ensuring the survival of cell cultures to undergo mucociliary differentiation. The time

course will also identify the threshold at which resubmerging cells leads to the detriment of the ALI cultures as seen in the ALI with no cilia condition.

Isolating cells from donor tissues provides a stable supply of affordable and consistent cells compared to commercially available ones; commercial cells have occurrences of bacterial and fibroblast contaminations. In contrast, cells isolated from tissues allow for the control of some aspects of these issues and provide a greater quantity of viable cells. However, they possess unique challenges. Despite few successes in propagating cells from the isolation to the model development stage, there are barriers to expanding these nasal epithelial cells. The most challenging aspect lies in culturing cells from the initial six-well plate to a T-25 flask because cells frequently die after being harvested and replated onto a larger growth surface area. Although attempts are made to overcome this obstacle, different methods fail to resolve this issue. One strategy includes plating harvested cells onto several wells in a six-well plate and cultured until 80% confluency before combining all the wells to replate into one T-25 flask. It has been suggested that antibiotic usage suppresses the growth and differentiation of primary cell cultures[41]. Since our tissue isolation protocol includes a 4% concentration of Primocin®, antibiotic use may account for the persistent difficulty in expanding the cells. The issue may have also arisen from the lack of reattachment from detached keratinocytes onto the six-well transwells and T-25 flasks. Collagen coating has been shown to enhance the attachment and growth of human keratinocytes[42] and may potentially mitigate the issue of reattachment. Future experiments will investigate the propagation of cells in collagen-coated flasks and the reduction of antibiotics in isolating cells from donor tissues to enhance yield and cell viability. Nonetheless, I have established two methods of isolating cells that

developed into a nasal organotypic model with goblet cell formation, an essential part of the epithelium reported in other primary ALI models[17,29], and visual ciliary motion.

In summary, we have established a method of obtaining a constant supply of cells through the approved clinical study and generated two protocols to isolate HpNECs successfully from donor tissues. We presented a differentiated nasal organotypic model using commercially available and locally isolated primary nasal epithelial cells. The presence of goblet cells and visually identifiable ciliated cells are characteristic of the pseudostratified columnar epithelium. Notably, we have shown that mucociliary differentiation was necessary to support SARS-CoV-2 infection. This finding underscores the importance of using primary epithelial cells to establish a differentiated culture for infection because cell lines like CALU-3 or HBEC-3KT do not exhibit mucociliary differentiation despite the presence of the ALI condition. Future work will create a time course of cell differentiation to verify the link between mucociliary differentiation and cell receptor polarization. In addition, this time course will also investigate the links between MUC5AC concentration and visual ciliary motion. Nonetheless, this established ALI differentiated model provides the fundamental basis for our future microbiota-viral-host interaction studies. With this model, we will look to incorporate the seven distinct CSTs in co-culture with the nasal model to investigate the effects of the microbiome on susceptibility to respiratory pathogens.

## Acknowledgements

We want to sincerely thank all tissue donors. Thanks to our collaborators for providing their assistance with the project and a huge thanks to my supervisor for their guidance and support. Finally, thank you to my lab members for their continued help throughout the year.

## References


1. Samarkos, M., Mastrogianni, E. & Kampouropoulou, O. The role of gut microbiota in Clostridium difficile infection. *Eur. J. Intern. Med.* **50**, 28–32 (2018).
2. Liu, C.M. *et al.* Penile Anaerobic Dysbiosis as a Risk Factor for HIV Infection. *mBio* **8**, e00906-17 (2017).
3. Fensterl, V. & Sen, G. C. Interferons and viral infections. *BioFactors Oxf. Engl.* **35**, 14–20 (2009).
4. Huan, Y., Kong, Q., Mou, H. & Yi, H. Antimicrobial Peptides: Classification, Design, Application and Research Progress in Multiple Fields. *Front. Microbiol.* **11**, (2020).
5. Benam, K. H., Vladar, E. K., Janssen, W. J. & Evans, C. M. Mucociliary Defense: Emerging Cellular, Molecular, and Animal Models. *Ann. Am. Thorac. Soc.* **15**, S210–S215 (2018).
6. Liu, Q. *et al.* Staphylococcus epidermidis Contributes to Healthy Maturation of the Nasal Microbiome by Stimulating Antimicrobial Peptide Production. *Cell Host Microbe* **27**, 68-78.e5 (2020).
7. Kim, H. J. *et al.* Nasal commensal Staphylococcus epidermidis enhances interferon-λ-dependent immunity against influenza virus. *Microbiome* **7**, 80 (2019).
8. Tsang, T. K. *et al.* Association Between the Respiratory Microbiome and Susceptibility to Influenza Virus Infection. *Clin. Infect. Dis. Off. Publ. Infect. Dis. Soc. Am.* **71**, 1195–1203 (2020).
9. Liu, C.M. & Voynow, J.A. Staphylococcus aureus and the ecology of the nasal microbiome. *Sci Adv.* **1,** e1400216 (2015).
10. Rose, M. C. & Voynow, J. A. Respiratory tract mucin genes and mucin glycoproteins in health and disease. *Physiol. Rev.* **86**, 245–278 (2006).

11. Linden, S. K., Sutton, P., Karlsson, N. G., Korolik, V. & McGuckin, M. A. Mucins in the mucosal barrier to infection. *Mucosal Immunol.* **1**, 183–197 (2008).
12. Buisine, M. P. *et al.* Developmental mucin gene expression in the human respiratory tract. *Am. J. Respir. Cell Mol. Biol.* **20**, 209–218 (1999).
13. Hovenberg, H. W., Davies, J. R. & Carlstedt, I. Different mucins are produced by the surface epithelium and the submucosa in human trachea: identification of MUC5AC as a major mucin from the goblet cells. *Biochem. J.* **318 ( Pt 1)**, 319–324 (1996).
14. Kesimer, M. *et al.* Tracheobronchial air-liquid interface cell culture: a model for innate mucosal defense of the upper airways? *Am. J. Physiol.-Lung Cell. Mol. Physiol.* **296**, L92–L100 (2009).
15. Kuek, L. E. & Lee, R. J. First contact: the role of respiratory cilia in host-pathogen interactions in the airways. *Am. J. Physiol. Lung Cell. Mol. Physiol.* **319**, L603–L619 (2020).
16. Lee, M.-K. *et al.* Air-liquid interface culture of serially passaged human nasal epithelial cell monolayer for in vitro drug transport studies. *Drug Deliv.* **12**, 305–311 (2005).
17. Charles, D. D. *et al.* Development of a Novel ex vivo Nasal Epithelial Cell Model Supporting Colonization With Human Nasal Microbiota. *Front. Cell. Infect. Microbiol.* **9**, 165 (2019).
18. Ahn, J. H. *et al.* Nasal ciliated cells are primary targets for SARS-CoV-2 replication in the early stage of COVID-19. *J. Clin. Invest.* **131**, e148517.
19. Jia, H. P. *et al.* ACE2 receptor expression and severe acute respiratory syndrome coronavirus infection depend on differentiation of human airway epithelia. *J. Virol.* **79**, 14614–14621 (2005).

20. Martens, K., Hellings, P. W. & Steelant, B. Calu-3 epithelial cells exhibit different immune and epithelial barrier responses from freshly isolated primary nasal epithelial cells in vitro. *Clin. Transl. Allergy* **8**, 40 (2018).
21. Kreft, M. E. *et al.* The characterization of the human nasal epithelial cell line RPMI 2650 under different culture conditions and their optimization for an appropriate in vitro nasal model. *Pharm. Res.* **32**, 665–679 (2015).
22. Grainger, C. I., Greenwell, L. L., Lockley, D. J., Martin, G. P. & Forbes, B. Culture of Calu-3 cells at the air interface provides a representative model of the airway epithelial barrier. *Pharm. Res.* **23**, 1482–1490 (2006).
23. Stadler, G. *et al.* Establishment of clonal myogenic cell lines from severely affected dystrophic muscles - CDK4 maintains the myogenic population. *Skelet. Muscle* **1**, 12 (2011).
24. Shen, B. Q., Finkbeiner, W. E., Wine, J. J., Mrsny, R. J. & Widdicombe, J. H. Calu-3: a human airway epithelial cell line that shows cAMP-dependent Cl- secretion. *Am. J. Physiol.* **266**, L493-501 (1994).
25. Moore, G. E. & Sandberg, A. A. STUDIES OF A HUMAN TUMOR CELL LINE WITH A DIPLOID KARYOTYPE. *Cancer* **17**, 170–175 (1964).
26. Moorhead, P. S. Human tumor cell line with a quasi-diploid karyotype (RPMI 2650). *Exp. Cell Res.* **39**, 190–196 (1965).
27. Lodes, N. *et al.* Investigation on Ciliary Functionality of Different Airway Epithelial Cell Lines in Three-Dimensional Cell Culture. *Tissue Eng. Part A* **26**, 432–440 (2020).
28. Ong, H. X. *et al.* Primary Air-Liquid Interface Culture of Nasal Epithelium for Nasal Drug Delivery. *Mol. Pharm.* **13**, 2242–2252 (2016).

29. Luengen, A. E. *et al.* Choosing the Right Differentiation Medium to Develop Mucociliary Phenotype of Primary Nasal Epithelial Cells In Vitro. *Sci. Rep.* **10**, 6963 (2020).
30. Pezzulo, A. A. *et al.* The air-liquid interface and use of primary cell cultures are important to recapitulate the transcriptional profile of in vivo airway epithelia. *Am. J. Physiol.-Lung Cell. Mol. Physiol.* **300**, L25–L31 (2011).
31. Kreimendahl, F. *et al.* Combination of vascularization and cilia formation for three-dimensional airway tissue engineering. *J. Biomed. Mater. Res. A* **107**, 2053–2062 (2019).
32. Hou, Y. J. *et al.* SARS-CoV-2 Reverse Genetics Reveals a Variable Infection Gradient in the Respiratory Tract. *Cell* **182**, 429-446.e14 (2020).
33. Roy, J. G., McElhaney, J. E. & Verschoor, C. P. Reliable reference genes for the quantification of mRNA in human T-cells and PBMCs stimulated with live influenza virus. *BMC Immunol.* **21**, 4 (2020).
34. Peabody, J. E. *et al.* Seeing cilia: imaging modalities for ciliary motion and clinical connections. *Am. J. Physiol. Lung Cell. Mol. Physiol.* **314**, L909–L921 (2018).
35. Leung, C., Wadsworth, S. J., Yang, S. J. & Dorscheid, D. R. Structural and functional variations in human bronchial epithelial cells cultured in air-liquid interface using different growth media. *Am. J. Physiol. Lung Cell. Mol. Physiol.* **318**, L1063–L1073 (2020).
36. Janke, C. & Montagnac, G. Causes and Consequences of Microtubule Acetylation. *Curr. Biol.* **27**, R1287–R1292 (2017).
37. Eshun-Wilson, L. *et al.* Effects of α-tubulin acetylation on microtubule structure and stability. *Proc. Natl. Acad. Sci. U. S. A.* **116**, 10366–10371 (2019).

38. Stewart, C. E., Torr, E. E., Mohd Jamili, N. H., Bosquillon, C. & Sayers, I. Evaluation of differentiated human bronchial epithelial cell culture systems for asthma research. *J. Allergy* **2012**, 943982 (2012).
39. Poumay, Y. & Pittelkow, M. R. Cell density and culture factors regulate keratinocyte commitment to differentiation and expression of suprabasal K1/K10 keratins. *J. Invest. Dermatol.* **104**, 271–276 (1995).
40. Spungin, B. & Silberberg, A. Stimulation of mucus secretion, ciliary activity, and transport in frog palate epithelium. *Am. J. Physiol.* **247**, C299-308 (1984).
41. Nygaard, U. H. *et al.* Antibiotics in cell culture: friend or foe? Suppression of keratinocyte growth and differentiation in monolayer cultures and 3D skin models. *Exp. Dermatol.* **24**, 964–965 (2015).
42. Yashiki, S., Umegaki, R., Kino-Oka, M. & Taya, M. Evaluation of attachment and growth of anchorage-dependent cells on culture surfaces with type I collagen coating. *J. Biosci. Bioeng.* **92**, 385–388 (2001).

## Figures and Tables

**Table 1. Clinical data for tissues collected for cell isolation**

| Study ID | Cell Isolation Date | Anatomical Location | Apparent Inflammation (Y/N) | Isolation Method (CO/Dispase) |
|---|---|---|---|---|
| HNEC_001 | Dec 31st 2021 | Posterior Septum | N | CO |
| HNEC_001 | Dec 31st 2021 | Superior Turbinate | N | CO |
| HNEC_001 | Dec 31st 2021 | Sphenoid | N | CO |
| HNEC_002 | Jan 6th 2022 | Uncinate/ethmoid | N | CO |
| HNEC_003 | Jan 13th 2022 | Uncinate/ethmoid | N | Dispase |
| HNEC_003 | Jan 13th 2022 | Maxillary Sinus | Y | Dispase |
| HNEC_004 | Feb 9th 2022 | Right uncinate bulla | N | Dispase + CO |
| HNEC_004 | Feb 9th 2022 | Left ethmoid bulla | N | Dispase + CO |
| HNEC_004 | Feb 9th 2022 | Right bulla | Y | Dispase + CO |
| HNEC_005 | March 5th 2022 | Middle Turbinate | N | Dispase + CO |

CO = Crawl-Out method

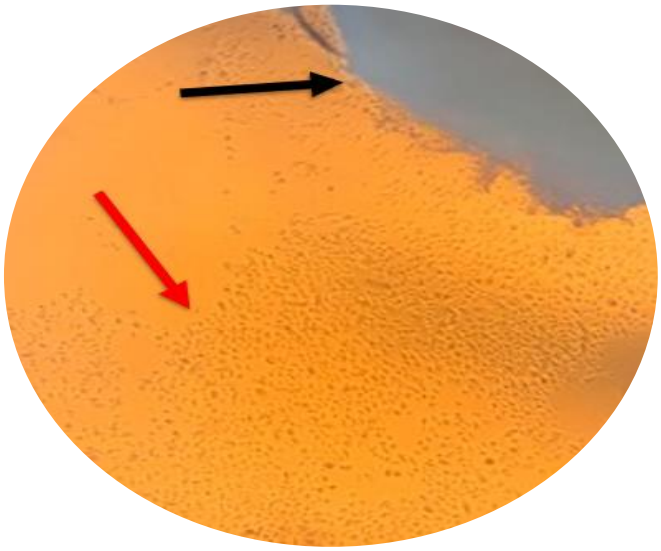

**Figure 1.** Human nasal epithelial cells migrating from donor tissues in the Crawl-Out method, study ID HNEC_001. To isolate human primary nasal epithelial cells (HpNECs), tissues were washed using phosphate-buffered saline (PBS) and processed into smaller pieces to adhere to a six-well plate. The black arrow indicates the donor tissue, and the red arrow points to the confluent cells surrounding the tissues at day 10 post cell isolation. Cells are ready to be harvested at this point and grown in a new well. The image was taken at 50x total magnification.

**Figure 2.** Human nasal epithelial cells isolated using the Dispase protocol from donor tissue, study ID HNEC_003. To isolate human primary nasal epithelial cells (HpNECs), tissues were processed into smaller pieces and incubated with dispase (1.8 U/ml) overnight at 4°C. Next, 10 mins incubation with 0.25% trypsin/EDTA for at 37°C with 5% CO2 supplemented air was performed and cells were collected by straining through a 70 μm cell strainer. Cells isolated using the Dispase method were ready to be passaged 3 days after the isolation protocol. The image was taken at 50x total magnification.

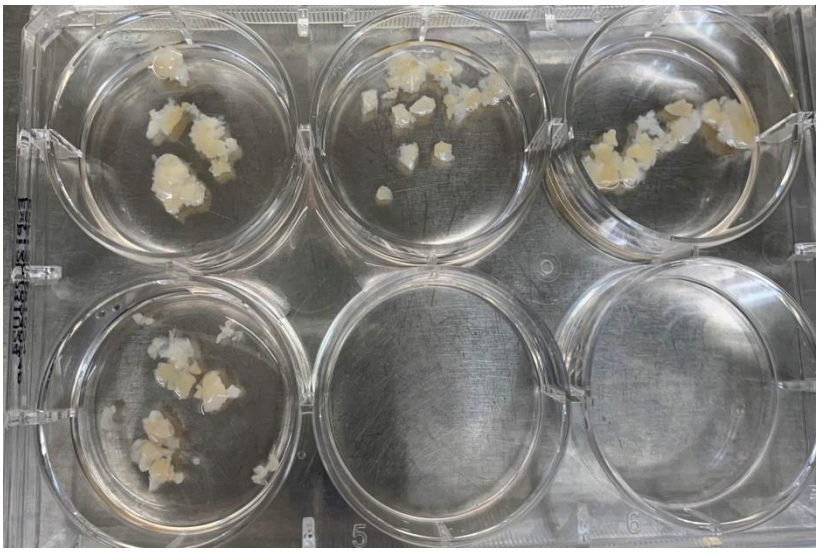

**Figure 3.** The combination of the Dispase method with the Crawl-Out method, study ID HNEC_005. To determine whether tissues that underwent the Dispase method could continue to produce epithelial cells, tissues were retained after the Dispase method. These tissues were allowed to adhere to the plate to begin the Crawl-Out protocol.

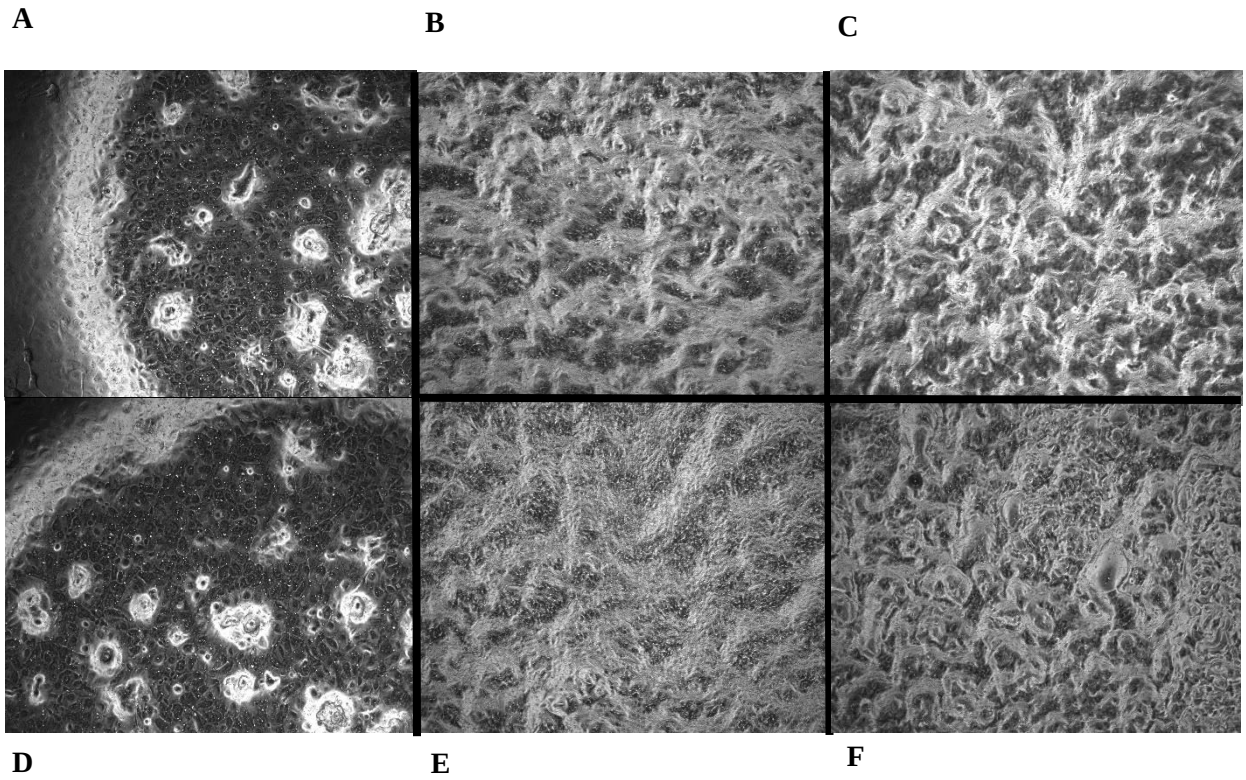


Figure 4. Topography of the primary nasal epithelial cells undergoing the air-liquid interface (ALI) condition. A) Human primary nasal epithelial cells (HpNECs) grown in 1-to-1 ratio of airway epithelial cells growth media (AECGM) and Dulbecco's Modified Eagle Medium (DMEM) at immediately after the introduction of ALI, b) at 14 days post-ALI, and C) at 21 days post-ALI. D) HpNECs grown in ALI differentiation media (Promocell) at 0 days post-ALI, E) at 14 days post-ALI, and F) at 21 days post-ALI. Images were taken at 50x total magnification.

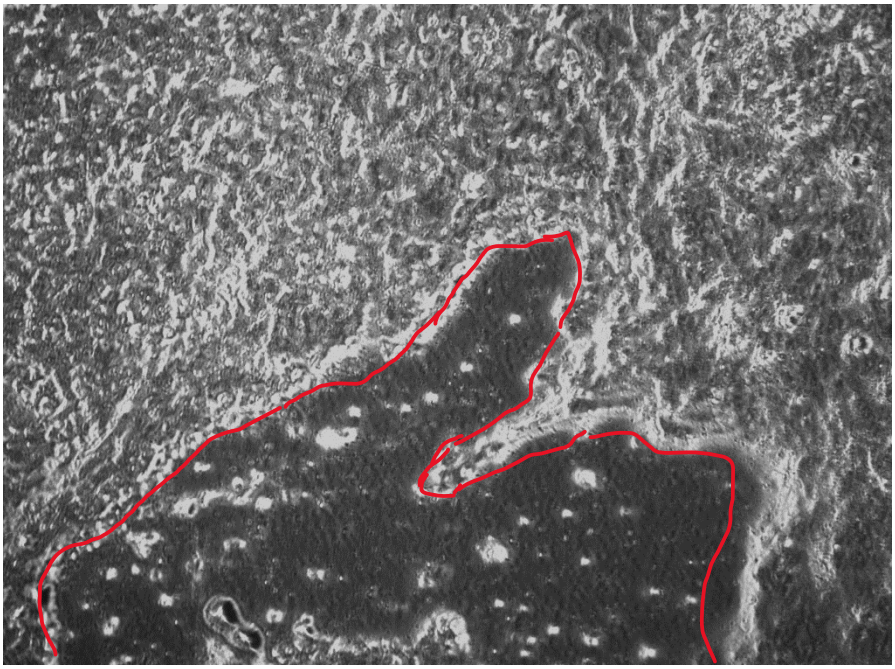

**Figure 5.** Human primary nasal epithelial cells were introduced to the air-liquid interface (ALI) condition. Cells that were prematurely introduced to the ALI condition prior to 100% confluency had gradual cell death shown as holes in the culture. As depicted by the red border, a patch of cells has been lost 7 days post-ALI. The image was taken at 50x total magnification.

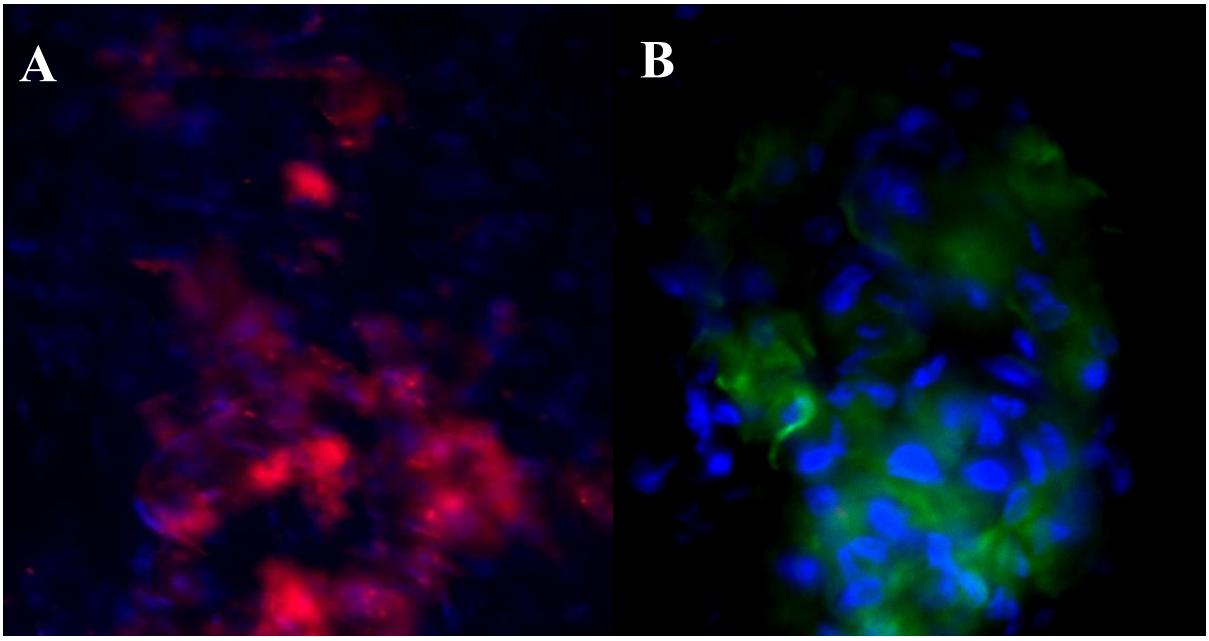


**Figure 6.** Immunofluorescence microscopy to access the differentiation state of cells that have undergone the air-liquid interface (ALI) condition. Cells in the ALI condition with visual ciliary motion on day 21 were fixed in 3.7% paraformaldehyde for 15 mins. A) In 1:400 dilution, Alexa Flour-647 conjugated MUC5AC antibodies were used to identify the presence of goblet cell differentiation. B) At 1:800 dilution, Alexa Flour-488 conjugated acetylated-alpha tubulin antibodies were used to stain for cilia shown in green. Fluoromount G mounting media with DAPI was used to counterstain nuclei shown in blue. Images were taken at 20x magnification.

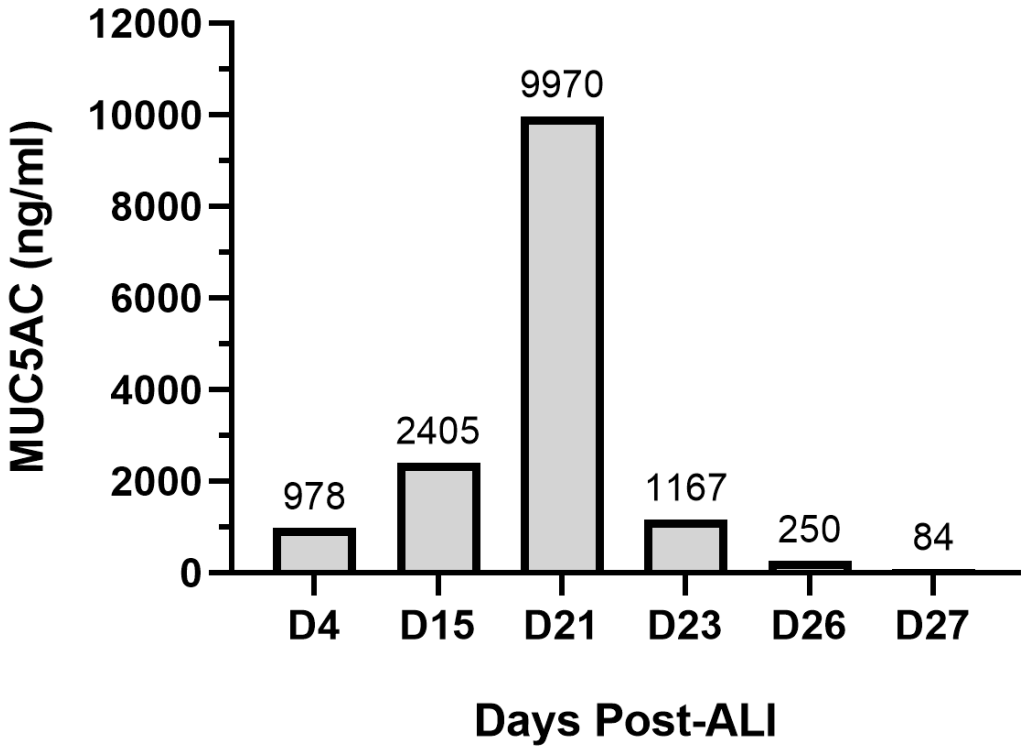


**Figure 7.** MUC5AC concentration as a function of days post-introduction of the air-liquid interface (ALI). 40 µl of phosphate-buffered saline (PBS) was added to the apical surface of the transwell and incubated for 5 mins to collect mucus secretion throughout the ALI condition. Collected samples were diluted to a total of 400-fold, and a MUC5AC enzyme-linked immunosorbent assay was performed to detect the presence of goblet cell formation. The concentration of MUC5AC increases gradually before peaking at day 21 post-ALI. Bars represent 1 sample collected from an ALI condition with the presence of visual ciliary beating.

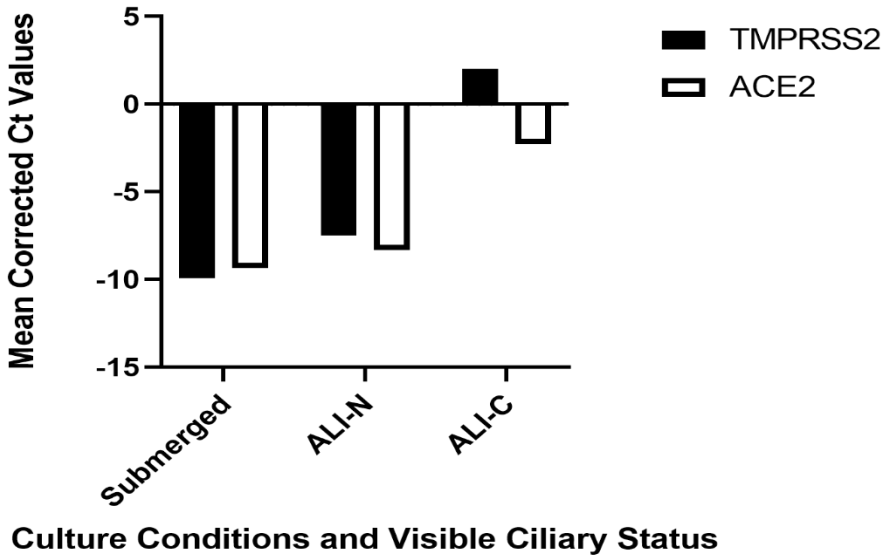


**Figure 8.** Mean corrected Ct values of TMPRSS2 and ACE2 expression in three different conditions. Cells from two wells were collected to create one sample for a total of n=2 for each condition at day 21 post-ALI. TaqMan expression assay was performed and normalized to the housekeeping gene, RSP-18. Air-liquid interface (ALI) model with visible ciliary motion under light microscopy (ALI-C) is shown to express angiotensin converting enzyme-2 (ACE2) and transmembrane serine protease 2 (TMPRSS2) higher compared to the ALI with no ciliary motion (ALI-N) and the submerged condition. Although the ALI-N condition has slightly higher expression of the two genes than the submerged model, the two conditions exhibit similar results. The bars represent the mean of the two samples corrected by the mean of the housekeeping gene.

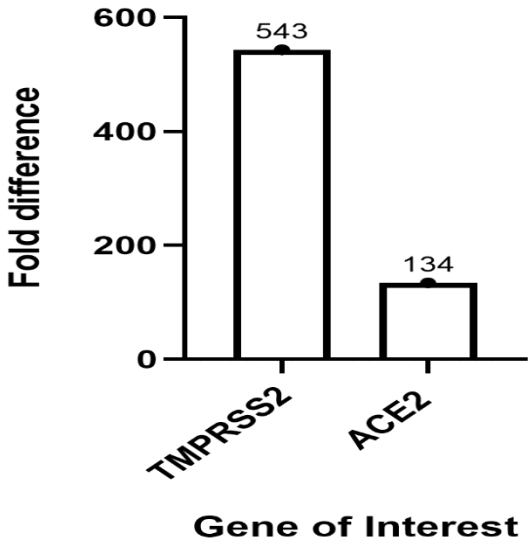


**Figure 9.** Fold differences in the expression of each gene in the air-liquid interface (ALI) condition compared to the submerged condition. Cells were collected from two wells to create one sample at day 21 post-ALI for n=2. TaqMan expression assay was performed and normalized to the housekeeping gene, RSP-18. There is a 543-fold increase in transmembrane serine protease 2 (TMPRSS2) expression and a 134-fold increase in angiotensin-converting enzyme 2 (ACE2) expression in the ALI condition compared to the submerged condition. The bars represent the fold difference of the mean corrected Ct values of 2 samples of the ALI condition compared to the submerged condition.

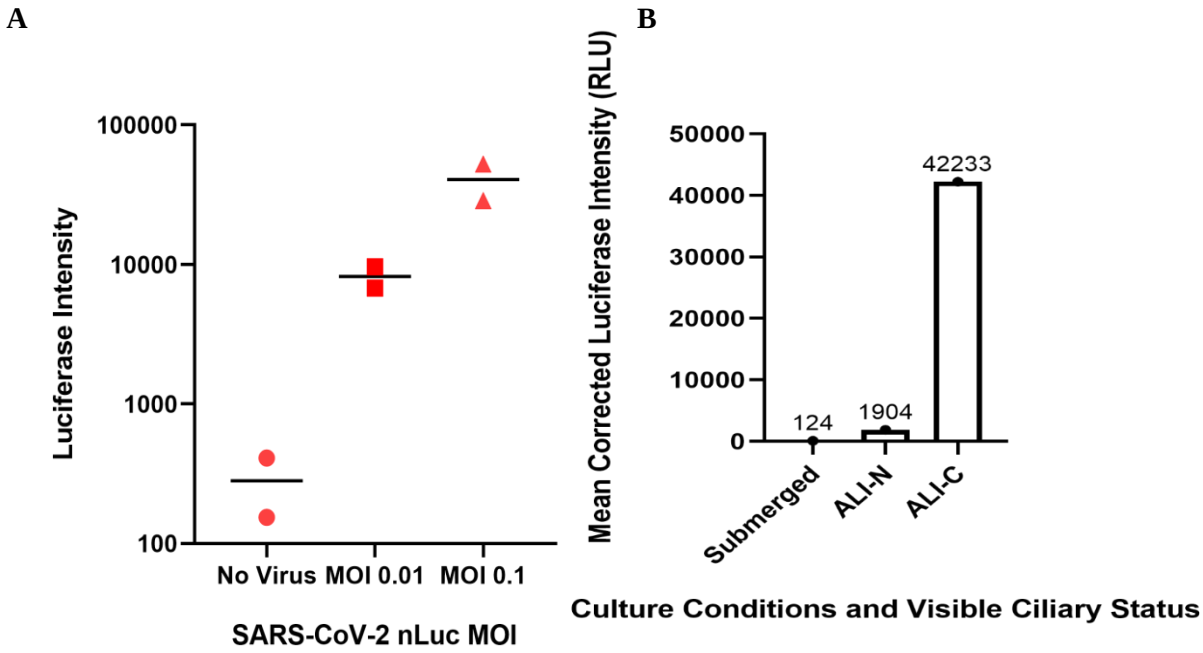


Figure 10. Viral challenge of three nasal models using wild-type severe acute respiratory syndrome coronavirus 2 (SARS-CoV-2) Nanoluciferase (nLuc). Infection was performed at day 26 post-ALI. A) Differentiated nasal models with ciliary motion were infected with SARS-CoV-2 with no virus, an MOI of 0.01, and an MOI of 0.1. The viral inoculum was incubated for 1 hour and wild-type SARS-CoV-2 nLuc was allowed to replicate for 3 days prior to measuring luciferase intensity as relative light units (N=2). B) At day 26 post-ALI, the submerged condition, the air-liquid interface (ALI) with no visual ciliary beating condition (ALI-N), and ALI with visual ciliary motion condition (ALI-C) were infected with SARS-CoV-2 nLuc. N=2 for the submerged and ALI-N condition and n=3 for the ALI-C condition. Compared to the models with no cilia, ALI-C condition had a large increase in luciferase intensity. The submerged and ALI-N condition are relatively similar in their poor ability to support viral infection. The bars represent the mean of the samples corrected by the mean of the no virus condition.

## Supplementary Materials

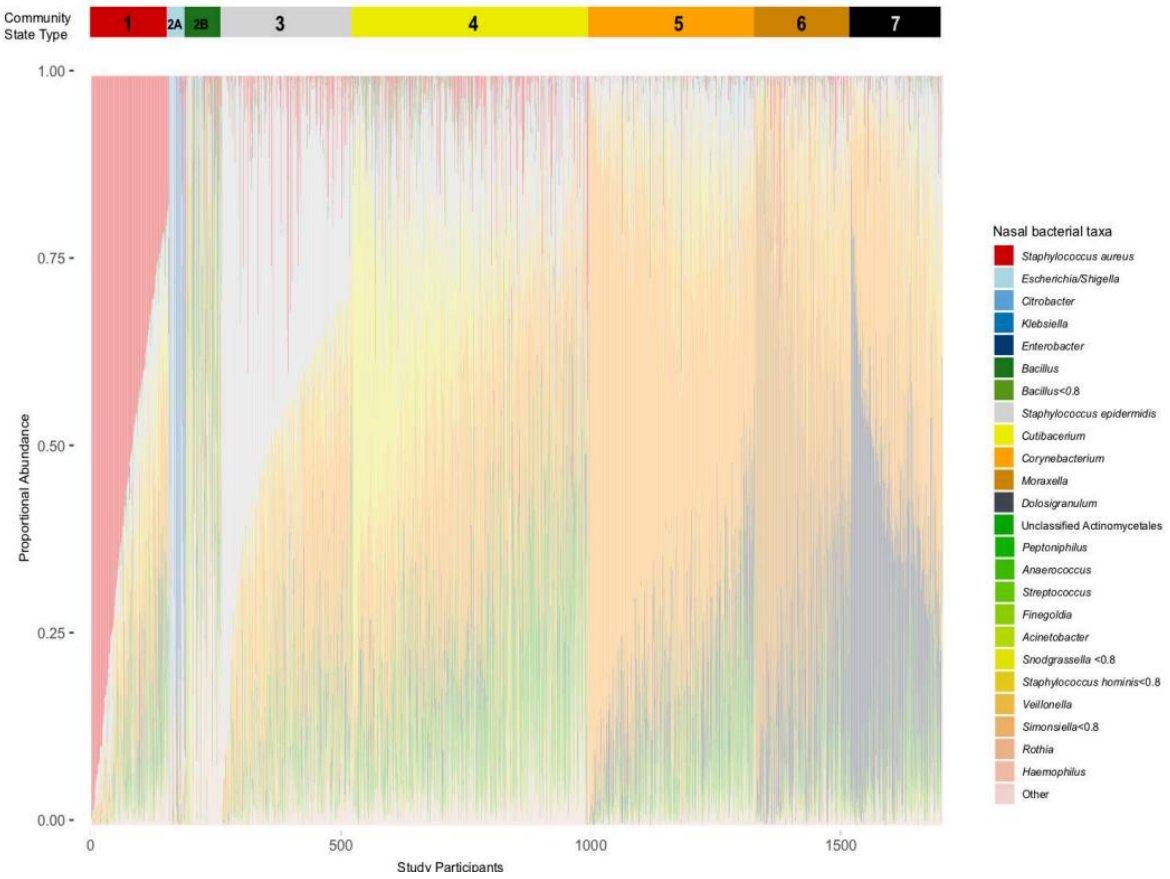


**Supplementary Figure 1**. Nasal microbiome profile identified as 7 distinct nasal community state types (CST) in Danish adults. The 7 CSTs include *S. aureus* (CST1; 9.0%), *Enterobacteriaceae* (CST2A; 2.1%), *Bacillus/Acinetobacter* (CST2B; 4.2%), *S. epidermidis* (CST3; 15.4%), *Cutibacterium* (CST4; 27.8%), *Corynebacterium* (CST5; 19.5%), *Moraxella* (CST6; 11.2%), *Dolosigranulum pigrum* (CST7; 10.8%). Figure provided by Dr. Cindy Liu from the George Washington University.

**Table 1.** Primers and probe sequence for ribosomal protein subunit 18 (RPS-18) housekeeping gene

| Gene | Forward Primer | Reverse Primer | Probe |
|---|---|---|---|
| RPS-18 | GTTCCAGCATATTTTGCGAGT | GTCAATGTCTGCTTTCCTCAAC | /5HEX/TCTTCGGCC/ZEN/CACACCCTTAATGG/3IABkFQ/ |